MethodsX 14 (2025) 103414

Contents lists available at ScienceDirect

MethodsX

journal homepage: www.elsevier.com/locate/methodsx

A method to map real-time gamma-ray radiation in urban areas near the soil surface ☆

Paulo Pereira [a,*], Luis Pinto [a], Miguel Inacio [a], Damia Barcelo [b], Eric C. Brevik [c], Corinne E. Brevik [d]

[a] Environmental Management Laboratory, Mykolas Romeris University, Vilnius, Lithuania
[b] Department of Chemistry and Physics, University of Almería, Spain
[c] School of Agricultural Sciences and School of Earth Systems and Sustainability, Southern Illinois University, Carbondale, IL, USA
[d] School of Physics and Applied Physics, Southern Illinois University, Carbondale, IL, USA

ARTICLE INFO

Method name:
Radiation mapping in urban areas

Keywords:
Radiation
Count rate
Dose rate
Land use
Spatial analysis

ABSTRACT

Radiation exists naturally in the environment. However, human activities, especially those related to nuclear weapons, energy generation, and medical infrastructures, can increase radioactivity levels in air, soil, and water, threatening human health. Both urban and rural populations can be exposed to radioactivity, making mapping an essential tool for a better understanding of radiation concentration. In this work, we developed a "walk-borne" survey methodology to map real-time gamma radiation (count and dose rate) in an urban area (Vilnius, Lithuania) using a small portable spectrometer (RadiaCode). A detailed method was developed considering 1) RadiaCode test in the field, 2) study site selection, 3) transect design to map count and dose rate, 4) RadiaCode map settings preparation, 5) fieldwork and data preparation, 6) data download and processing, and 7) statistical and spatial analysis. This method will be key to identifying potential radiation sources and accumulation that can be transferable to other environments.

- A novel "walk-borne" survey methodology was developed to map real-time gamma-ray radiation using a small portable spectrometer;
- High-resolution mapping of potential radiation sources can be identified with their implications for human health
- This method can help identify areas with potential radiation risks.

Specifications table

Subject area:	Environmental Science
More specific subject area:	*Environmental radiation; Mapping*
Name of your method:	*Radiation mapping in urban areas*
Name and reference of original method:	*Not applicable*
Resource availability:	*Detector of nuclear radiation and spectrometer Radiacode 103.* *Computer Intel(R) Core (TM) i9-10900X CPU @ 3.70GHz 3.70 GHz and 64.0 GB Memory* *Google Earth Online* *RadiaCode Application* *ArcGIS Pro (ver. 3.1.2)* *JASP 0.18.3.0*

☆ **Related research article:** None.

* Corresponding author.
E-mail address: paulo@mruni.eu (P. Pereira).

https://doi.org/10.1016/j.mex.2025.103414
Received 27 April 2025; Accepted 2 June 2025
Available online 3 June 2025
2215-0161/© 2025 The Author(s). Published by Elsevier B.V. This is an open access article under the CC BY-NC-ND license (http://creativecommons.org/licenses/by-nc-nd/4.0/)

Background

Radiation is defined as energy that moves from one place to another in the form of electromagnetic waves or particles. Electromagnetic (EM) radiation describes energy which is transmitted in the form of light waves or photons, examples of which include ultraviolet light which is emitted by the sun, x-ray photons which are used in medical diagnostics, and gamma rays that can be used to treat certain types of cancers. Nuclear radiation refers to energy released when the nucleus of an atom either transmutates (changes its identity) or de-excites, and the energy can be carried by several different types of particles, including neutrons, alpha particles, beta particles, or gamma rays.[1]

Radiation exists naturally in the environment, coming from space (e.g. cosmic rays) and terrestrial (e.g., rocks, soil) sources. Gamma rays are released during the decay of naturally-occurring isotopes such as potassium-40, thorium-232, uranium-238, and lutetium-176. Other isotopes such as cesium-137, cobalt-57 and americium-241 are of anthropogenic origin and can be released into the environment from nuclear reactors, industrial and military activities, power generation, construction activities, and medical facilities [1–3]. High concentrations of these isotopes in the environment can harm human health, particularly in urban areas with higher population density [4,5]. Radiation can exist within the human body due to ingestion or inhalation of radioactive sources such as radon gas, soils, tobacco, or certain foods [6–8]. Gamma rays can travel longer distances through the air and penetrate further into a tissue than other forms of radiation, provoking significant body damage [9–12].

Various quantities have been developed throughout the years to quantify both the amount of radiation that has been absorbed by an object as well as the amount of damage that the radiation can inflict on different types of tissue. *Exposure* measures the amount of charge that is separated when radiation particles ionize a mass of air; a common unit for exposure is the roentgen [R]. *Absorbed dose* measures the energy per mass deposited into a substance; units for absorbed dose include the gray [Gy] and the radiation-absorbed-dose [rad]. The *equivalent dose* considers both the energy per mass deposited into a substance as well as the type of radiation that was absorbed by including a radiation weighting factor; it is measured in sieverts [Sv] or roentgen-equivalent-man [rem]. The *effective dose* adjusts the equivalent dose by a tissue weighting factor to account for the varying sensitivities of different organs to radiation damage; it is also measured in Sv or rem [13].

After the Chernobyl nuclear disaster in 1986, large areas of Eastern and Central Europe and Asia were contaminated with cesium-137, strontium-90, iodine-131, and plutonium-241. Although the major impacts in the environment were identified in European Russia, Belarus, and Ukraine, other countries such as Lithuania, Poland, Romania, Sweden, Finland, Georgia, Armenia, and Turkey were also affected. These countries may still have problems with radiation to the present day [14–17].

Mapping is fundamental to understanding environmental phenomena [18]. Several works have focused on mapping radiation concentrations [19,20] using different technologies such as unmanned aerial vehicles [21] or gamma-ray spectrometers [22] in the field. This is a fundamental key to identifying areas of natural and anthropogenic radiation sources that can harm human health and emergency perparedeness. Environmental radiation depends on several factors such as rock properties, atmospheric pressure, rainfall, relative humidity, wind speed and temperature, and soil properties such as water content, salinity, and total organic matter [23–26]. Therefore, it is important to measure natural (e.g., rock type, soil properties and meteorological conditions) and anthropogenic (e.g., proximity to health care facilities, types of industrial infrastructure, building materials used) factors to understand what affects radiation concentration. This requires many samples, and conventional radiation analysis is costly and time-consuming. Although using portable spectrometers to measure radiation in situ cannot completely replace conventional laboratory analysis [27], they can identify areas affected by radiation much more quickly. This is key to finding areas that potentially have high radiation levels. In this context, it is essential to establish monitoring programs that consider quick assessments to collect radiation data important for decision-making [28]. Multiple works have been conducted in situ to map radiation concentrations that are linked to a GIS database [29,30].

Recently a small and portable spectrometer, RadiaCode[2], was released in the market. It is considered the next-generation “Geiger counter” since it can collect data faster than traditional Geiger counters. It can also identify radiation sources and the isotopes released, which gives it tremendous promise as a monitoring tool, and it is relatively inexpensive. Among other novel features, data can be recorded using a GPS tracker and mapped in real-time. This represents a tremendous advance in identifying potential radiation sources. Furthermore, due to its ease of use and low cost, it is ideal for potential incorporation into future citizen science projects. Radiation has been successfully tracked in the past using citizen science, particularly after the Fukushima event [31,32]. In this work, we aim to develop a robust methodology to map air radiation near the soil surface (count and dose rate) in Vilnius, the capital of Lithuania, a country strongly affected by the Chernobyl nuclear disaster [33]. In urban environments, streets, lawns, roads, parks, or squares can be contaminated with radionuclides [14]; therefore, assessing radiation in different urban land uses is important. To do this, we developed a “walk-borne” survey methodology to measure ambient radiation using a portable radiation detector (RadiaCode) to measure ambient gamma radiation from terrestrial sources. This will be important for geochemical exploration and dose mapping at large scale, and can potentially be utilized in citizen science studies to increase areas of coverage.

[1] https://www.iaea.org/newscenter/news/what-is-radiation.

[2] https://www.radiacode.com/eur?srsltid=AfmBOornQQS_XIIIAKcnNRgt_m6_xWKCswD9Zo0pyexFHZx-7XGro0dI.

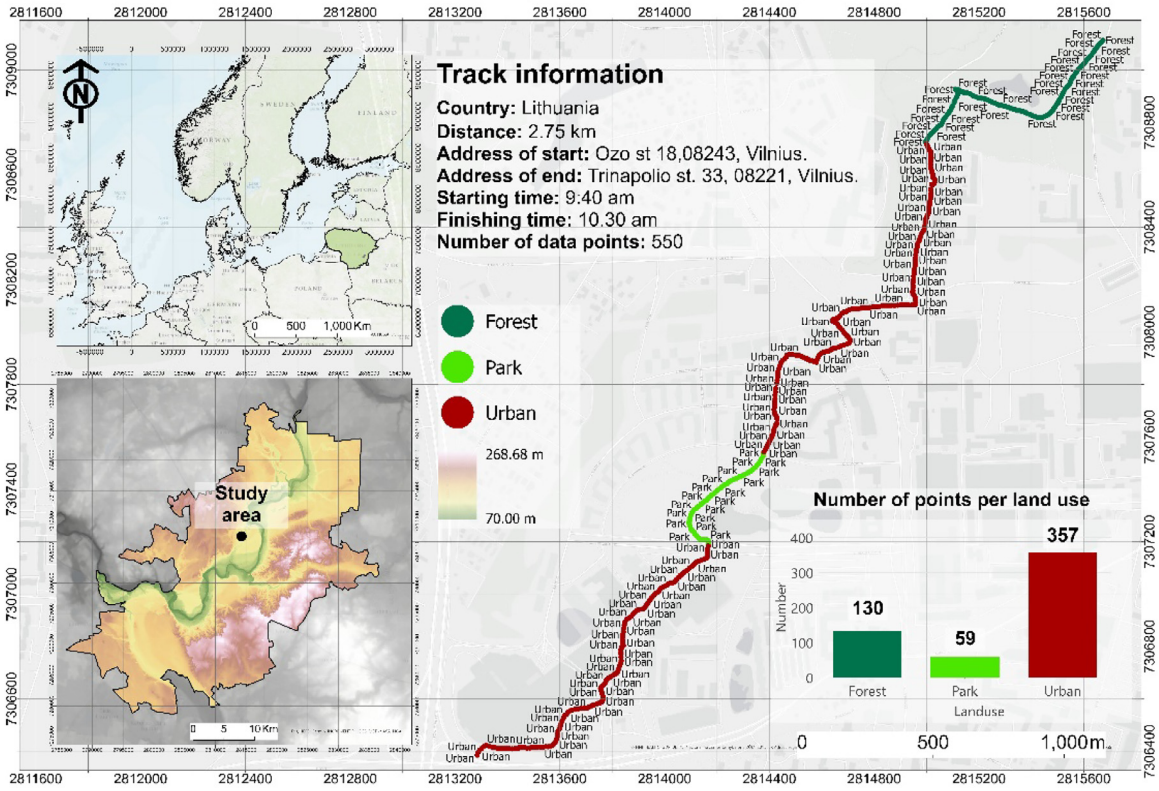


Fig. 1. Study area.

Method details

Application download and device test

The area where the method was tested is shown in Fig. 1. Before establishing the experimental design and testing the RadiaCode 103 (specifications described in Table S1), the mobile application needed to map air radiation concentration was downloaded from the Google Play Store[3] (Fig. 2). The most up-to-date version available at the time of the study (1.63.02) was used. The application was installed on a Xiaomi Redmi Pad SE 8.7 (specifications described in Table S2). The RadiaCode application can be installed on Android and IOS (Apple) devices. However, the Android version is more developed, which is why it was chosen for this study.

The RadiaCode 103 measures both count rate and equivalent dose rate.[4] The count rate measures the number of radiation decays per minute (cpm) or per second (cps). Normally, the count rate decreases with increasing distance to the source. The higher the counts, the higher the radiation emission of one or more radioactive isotopes. The RadiaCode measures the dose in rem, R, and Sv. This work measured radiation in microroentgen per hour (μR/h).

The RadiaCode 103 device can also identify the isotopes responsible for radiation emission, which was only previously possible using expensive laboratory instruments. The RadiaCode website has an isotopes spectrum library that is very useful for determining the characteristics of the different isotopes and the spectrum they are identified by.[5] This is a great advance in radiation analysis; it allows us to focus on the RadiaCode 103 as a potential rapid and inexpensive mapping tool.

Before establishing the experimental design, we tested the device in the field along several tracks and investigated the different features of the RadiaCode application, including sampling distance, walking velocity, and crossing roads. This was essential to sample data in the same areas during different sampling periods. Previous to each test and measurement, the RadiaCode 103 was calibrated using a WT-20 Red TIG Welding Tungsten Electrode following the steps specified on the RadiaCode website.[6]

[3] https://play.google.com/store/apps/details?id=com.almacode.radiacode&hl=en_US&pli=1.
[4] https://coda.io/d/radiacode-cyberspace_dTtFtorf-v-/Quick-Guide-Manual_suS3AbP_.
[5] https://www.radiacode.com/eur/spectrum-isotopes-library.
[6] https://docs.radiacode.com/EN/Video+Tutorials/Calibration.

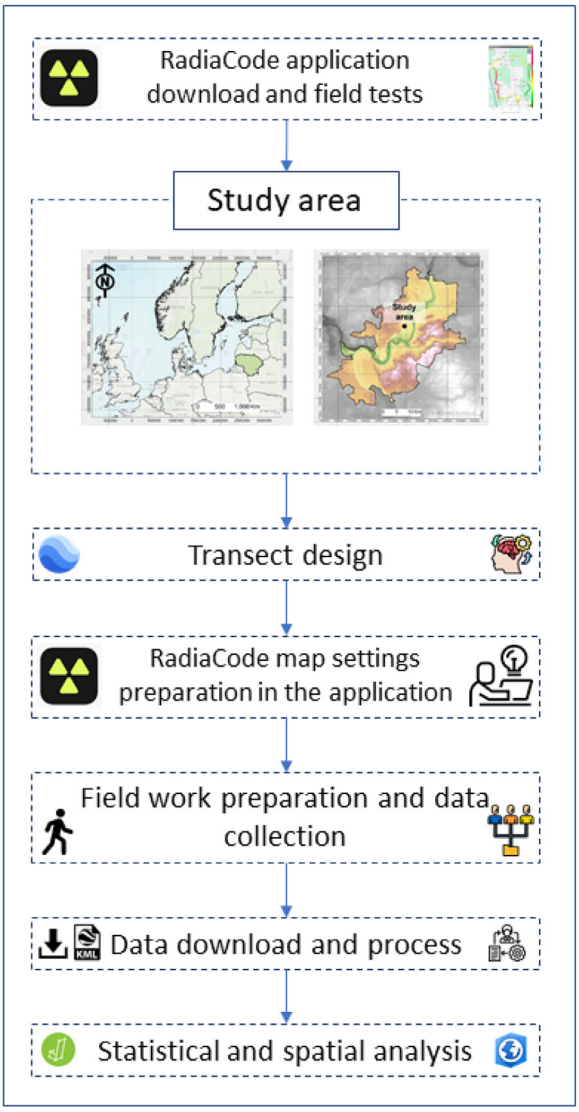


Fig. 2. Framework applied.

Track design and RadiaCode map settings preparation

A track was designed on Google Earth online[7] and a Keyhole Markup Language (KML) was created (Fig. 2). This file was converted to a shapefile using My Geodata[8] so it could be represented in ArcGIS Pro. It was important that the track would cross different land uses (forest, park and urban) and be easily walkable in a short time to avoid changes in environmental (e.g., temperature, humidity, wind) and anthropogenic (e.g., traffic) influences (Fig. 1). The track was 2.75 km long. Data collection was started at 9:40 am and finished at 10:30 am with 550 sample points. Before starting the measurements, several aspects needed to be considered. The RadiaCode 103 was placed on the right foot using an anklet (Figure S1) and was well-secured to avoid falling during data collection. The anklet was placed 20 cm above the soil surface. The RadiaCode was placed around the ankle as this was recommended on the RadiaCode webpage.[9] Previous works have also measured environmental gamma radiation at 20 cm height [34,35]. The general

[7] https://earth.google.com.
[8] https://mygeodata.cloud/converter/kml-to-shp.
[9] https://www.radiacode.com/eur/products?utm_term=&utm_campaign=&utm_source=adwords&utm_medium=ppc&hsa_acc=8003974282&hsa_cam=22367323633&hsa_grp=&hsa_ad=&hsa_src=x&hsa_tgt=&hsa_kw=&hsa_mt=&hsa_net=adwords&hsa_ver=3&gad_source=1&gad_campaignid=22367328475&gbraid=0AAAAAqGyHaXkOzre8Ate5yDCD_9bMJJCJ&gclid=CjwKCAjw3MXBBhAzEiwA0vLXQfIZNZtD9_NJ9YXhDVd-EoQjiiwm5ZjiJfLMGlqlHMPxexrISL9zURoCdZIQAvD_BwE#!/Leg-Band-for-Radiacode-10X/p/573759725.

settings of the RadiaCode 103 during the walk are shown in Table S4. The count rate was set as pulses per second, the dose rate was measured using R/s units, and data was collected at 5 m intervals. This distance was selected because the GPS unit had a resolution of ±2 m. The sampling distance was larger than the resolution, which can reduce the resolution error effect.

Data collection and processing

The RadiaCode Android application allows collection of the count and dose rate in real time (Fig. 2). The application also allows photos to be taken and linked with measurement points (Figure S2). This is an important feature since areas with high count or dose rate values can be identified for future inspection. After finishing the track, it is also possible to identify the maximum and minimum values in the application. Once data was collected, the RadiaCode Android application saved the data as a KML file, which was later exported as a shapefile using the same procedure applied to the track file. Once data was converted to a shapefile, it was assessed in ArcGIS Pro for spatial analysis. Data was exported as a dBase database file for statistical analysis in JASP 0.18.3[10] and later converted into a comma-separated values (CSV) file. Using the KML file created in the RadiaCode Android application and a background satellite image from September 2023 in Google Earth Pro, the measurement points were classified into forest (230), park (59), and urban areas (357) (Fig. 1). After this assessment the classifications were confirmed in the field, especially in the transitions between land uses.

Statistical and spatial analysis

We collected samples on a weekend (30 March 2025) and weekday (02 April 2025) at the same time (9:40-10:30 am) and under similar weather conditions (sunny) to minimize any effects that time of day or weather conditions might have on data collection. determine if count and dose rate were influenced by the different times of data collection. To understand data distribution, several descriptive statistical analyses were performed in JASP 0.18.3, including median and standard error, skewness, kurtosis, minimum, maximum, 25^{th}, and 75^{th} percentile. Data homogeneity and heteroscedasticity were assessed using the Kolmogorov-Smirnov and Leven's methods. Data was considered normal and the variances were heterogenic at $p<0.05$. Count and dose rate data were not normally distributed and were heteroscedastic. Therefore, comparisons between time and land uses were conducted using a non-parametric Kruskal-Wallis ANOVA. If significant differences were found at a $p<0.05$, the Dunn post-hoc test with Bonferroni correction was applied (Fig. 2).

Spatial analysis was conducted in ArcGIS Pro. Count and dose rate data were standardised using the ArcGIS Pro data engineering tool.[11] We applied the Min-Max method as a standardisation technique. This step is essential to reduce the effects of the outliers in spatial analysis. Data was mapped using the unclassed colours method.[12] Using the standardised data, the semivariogram was modelled for count and dose rate on 30 March 2025 and 02 April 2025 using ArcGIS Pro Geostatistical Wizard.[13] The semivariogram is a geostatistical tool that assesses the degree of data spatial correlation [36]. The semivariogram was modelled using the ordinary kriging method. In this work an isotropic semi-variogram was modeled that can be used in linear point data as conducted elsewhere [37,38]

The selected geostatistical parameters are shown in Table S7. Semivariogram structure was assessed with the nugget effect (data measurement error), range (the distance where the spatial correlation is observed) and the partial sill (sill minus the nugget effect).[14] The accuracy of the ordinary kriging method was assessed using the leave-one-out cross-validation method. To conduct this assessment in ArcGIS Pro, a shapefile was created with the data measured, predicted, error, standard error and standardised error information by running the Geostatistical Wizard. Using this information, it was possible to assess the model's performance using the root mean square error (RMSE) and the regression (R^2) between the measured and predicted. The lower the RMSE and the higher the R^2 the more accurate the model is.[15] Moran's *I* global autocorrelation test was applied to identify if the data had clustered, random, or dispersed patterns. Values with a Moran's *I* closer to +1 indicate that data has a clustered pattern, values near -1 that the pattern is dispersed, and values near 0 that data is randomly distributed.[16] The inverse distance was used to conceptualise spatial relationships as a distance method, the Euclidean distance and a row standardisation. The Getis-Ord Gi* was applied to identify areas with significant cold and hot spot analysis.[17] As conceptualisation of spatial relationships and distance, the parameters applied in Moran's I global autocorrelation test were applied here as well. If the obtained z-score is < -1.65 or > +1.65, there is a 90% probability that there is a cold or hot spot area.[18] Hot and cold spot analysis allowed us to identify high and low count and dose rate clusters. A cluster and outlier analysis (Anselin Local Moran's I)[19] was applied to identify spatial areas where clusters of high and low values and outliers can be identified within these areas. This analysis is important to assess data spatial variability. The parameters applied in Moran's *I*

[10] https://jasp-stats.org/.
[11] https://pro.arcgis.com/en/pro-app/latest/help/analysis/geoprocessing/data-engineering/what-is-data-engineering.htm.
[12] https://pro.arcgis.com/en/pro-app/latest/help/mapping/layer-properties/unclassed-colors.htm.
[13] https://pro.arcgis.com/en/pro-app/latest/help/analysis/geostatistical-analyst/get-started-with-geostatistical-analyst-in-arcgis-pro.htm.
[14] https://pro.arcgis.com/en/pro-app/latest/help/analysis/geostatistical-analyst/understanding-a-semivariogram-the-range-sill-and-nugget.htm.
[15] https://pro.arcgis.com/en/pro-app/latest/help/analysis/geostatistical-analyst/performing-cross-validation-and-validation.htm.
[16] https://pro.arcgis.com/en/pro-app/latest/tool-reference/spatial-statistics/spatial-autocorrelation.htm.
[17] https://pro.arcgis.com/en/pro-app/latest/tool-reference/spatial-statistics/hot-spot-analysis.htm.
[18] https://pro.arcgis.com/en/pro-app/latest/tool-reference/spatial-statistics/what-is-a-z-score-what-is-a-p-value.htm.
[19] https://pro.arcgis.com/en/pro-app/latest/tool-reference/spatial-statistics/cluster-and-outlier-analysis-anselin-local-moran-s.htm.

Table 1
Count and dose rate in the different sampling times.

	Count rate (cps)		Dose rate (μR/h)	
	30-03-2025	02-04-2025	30-03-2025	02-04-2025
N	550			
Median	5.130	4.885	7.050	7.150
KW test	p<0.001		p<0.001	
Skewness	-0.407	-0.166	-0.811	0.297
Kurtosis	-0.472	-1.112	-0.244	-0.051
Minimum	4.610	4.270	4.990	5.380
Maximum	5.480	5.320	8.100	9.310
25^{th} percentile	4.980	4.570	6.482	6.460
75^{th} percentile	5.238	5.050	7.530	7.558

Table 2
Count and dose rate in the different land uses. Significant letters represent significant differences at a p<0.05.

	Count rate (cps)			Dose rate (μR/h)		
	Forest	Park	Urban	Forest	Park	Urban
N	230	59	357	230	59	357
Median	5.110a	4.745c	5.005b	7.400a	6.180c	7.075b
KW test	p<0.001			p<0.001		
Std. Error	0.007	0.017	0.011	0.051	0.041	0.029
Skewness	-1.168	-0.759	-0.279	-1.262	0.328	0.112
Kurtosis	4.520	-0.639	-0.908	0.226	-0.579	0.463
Minimum	4.560	4.270	4.310	5.060	5.420	4.990
Maximum	5.330	4.980	5.480	7.890	7.220	9.310
25^{th} percentile	5.040	4.520	4.730	6.830	5.938	6.640
75^{th} percentile	5.180	4.800	5.190	7.600	6.543	7.550

Table 3
Geostatistical and variogram model results.

Semi-Variogram	30-03-2025		02-04-2025	
	Count rate	Dose rate	Count rate	Dose rate
Number of lags	12			
Lag size	0.00041			
Nugget effect	0.000731	0.00736	0.00265	0.00037
Model type	Spherical	Gaussian	Circular	Spherical
Range (Distance 10^{-3} degrees)	0.07525	0.00193	0.0036	0.0029
Partial sill	0.07455	0.07057	0.08714	0.05412

global autocorrelation test (conceptualisation of spatial relationships, distance and standardisation) were also applied in the cluster and outlier analysis (Anselin Local Moran's *I*). This analysis can assess the cluster/outlier type (COType). High-high values (HH) show there is a cluster with high values in the area, while low-low values (LL) are the opposite. An outlier with a high value surrounded by low values is represented as high-low values (HL). If the opposite occurs, the point(s) are represented as low-high values.[20]

Method results, validation, and limitations

The results of the method showed that the count and dose rate were significantly higher on 30-03-2025 (weekend) than on 02-04-2025 (weekday) (Table 1). The count and dose rates were highest in forest land use, followed by urban with park values being the lowest (Table 2). This is also visible in Figs. 3, 4, 5 and 6. The highest data variability was in urban areas and the lowest was in parks. The highest individual readings for count and dose rate were in the urban land use (Table 2). The semivariogram results are shown in Table 3 and Fig. 7. The nugget effect was reduced in all cases. The best-fit models for the 30-03-2025 count rate and 02-04-2025 dose rate were spherical, while for the dose rate on 30-03-2025 and count rate on 02-04-2025 the best-fit models were Gaussian and Circular. The range was highest for count rate and lowest for dose rate on 30-03-2025. Finally, the partial sill was lowest for the dose rate and highest for the count rate on the same date (02-04-2025). The cross-validation results are shown in Table 4 and Figure S3. Overall, the RMSE of all the models was low and the R^2 was very high (>0.90), showing that the measured values were similar to the predicted. The majority of the errors were located near 0. The Morans *I* global spatial autocorrelation showed that the count

[20] https://pro.arcgis.com/en/pro-app/latest/tool-reference/spatial-statistics/h-how-cluster-and-outlier-analysis-anselin-local-m.htm.

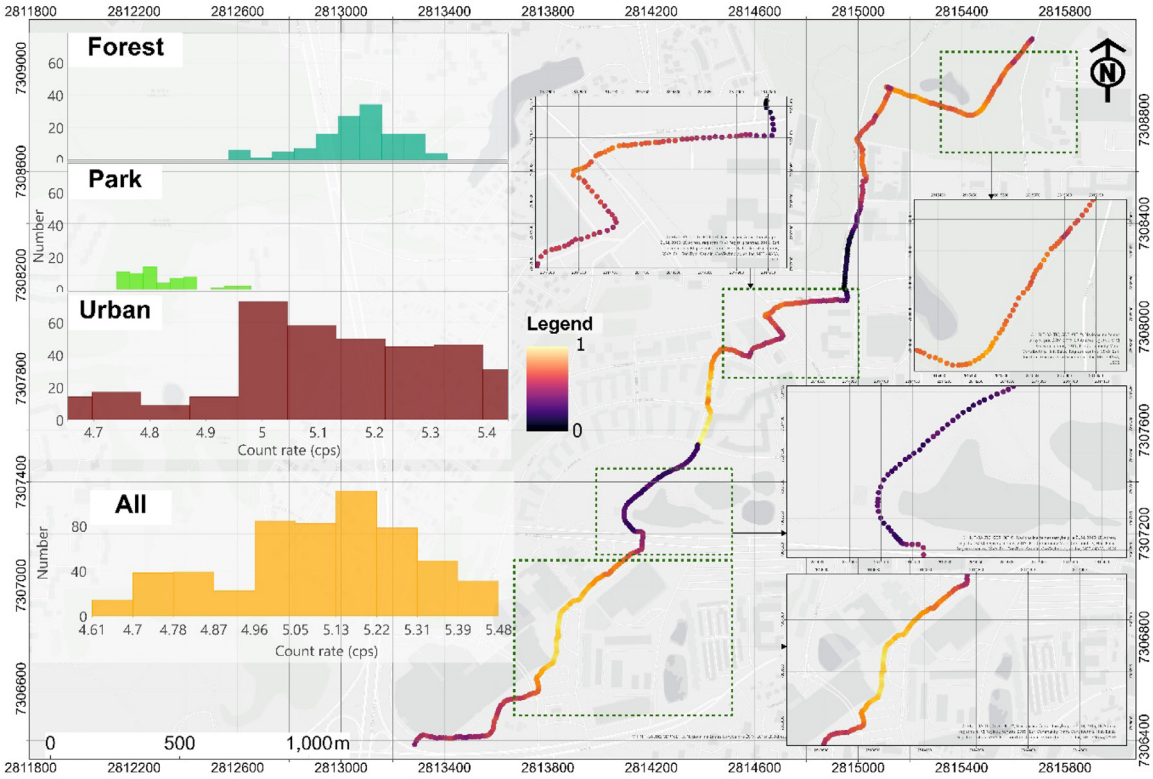


Fig. 3. Radiation count rate in the transect studied and the respective histograms according to land use in 30-03-2025.

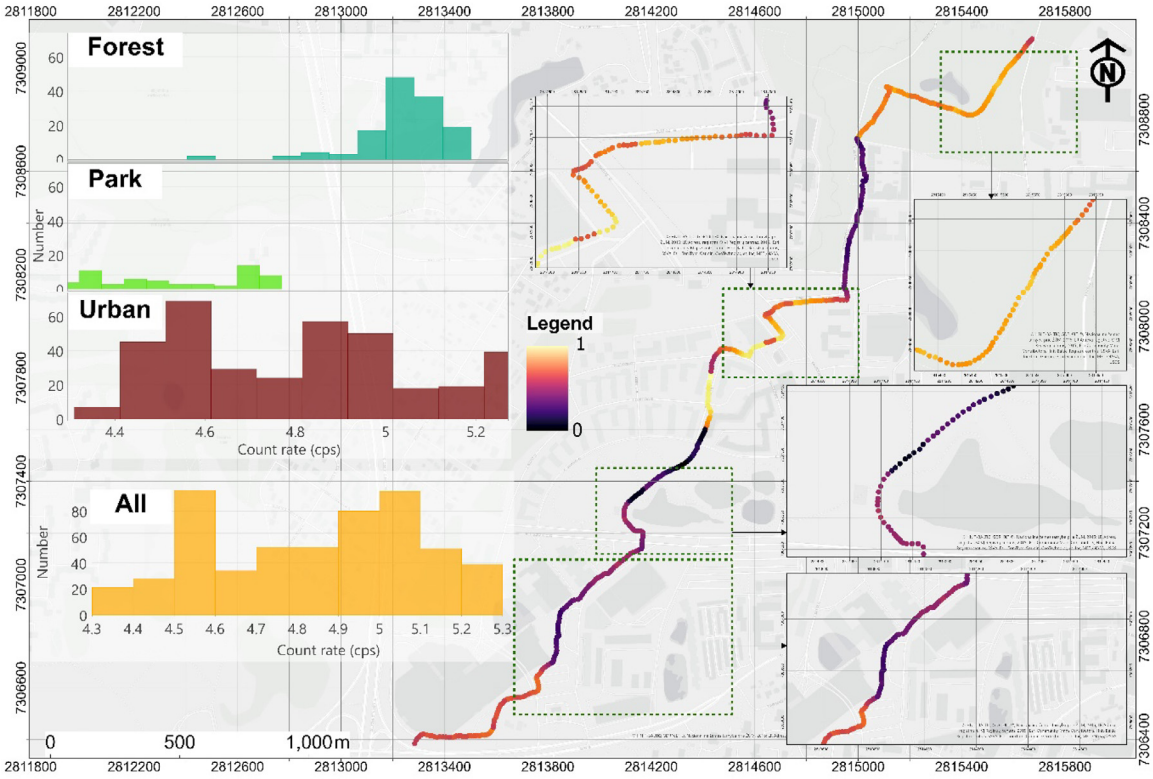


Fig. 4. Radiation count rate in the transect studied and the respective histograms according to land use in 02-04-2025.

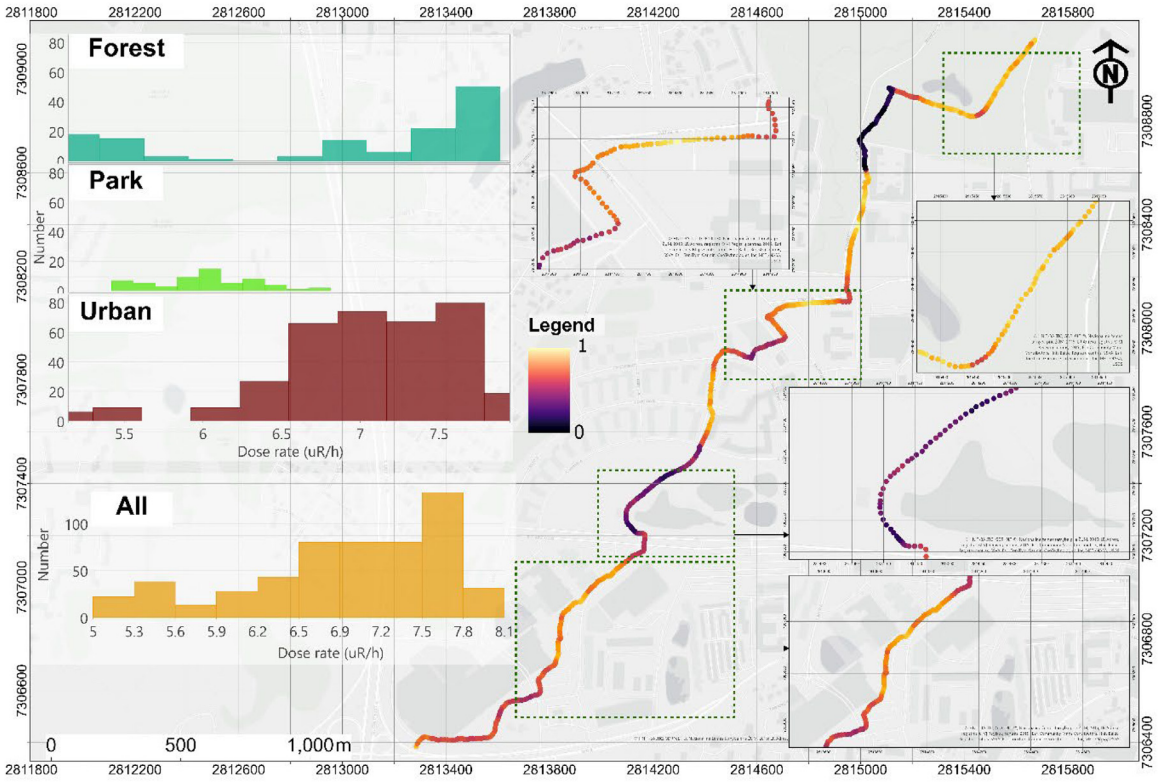


Fig. 5. Radiation dose rate in the transect studied and the respective histograms according to land use in 30-03-2025.

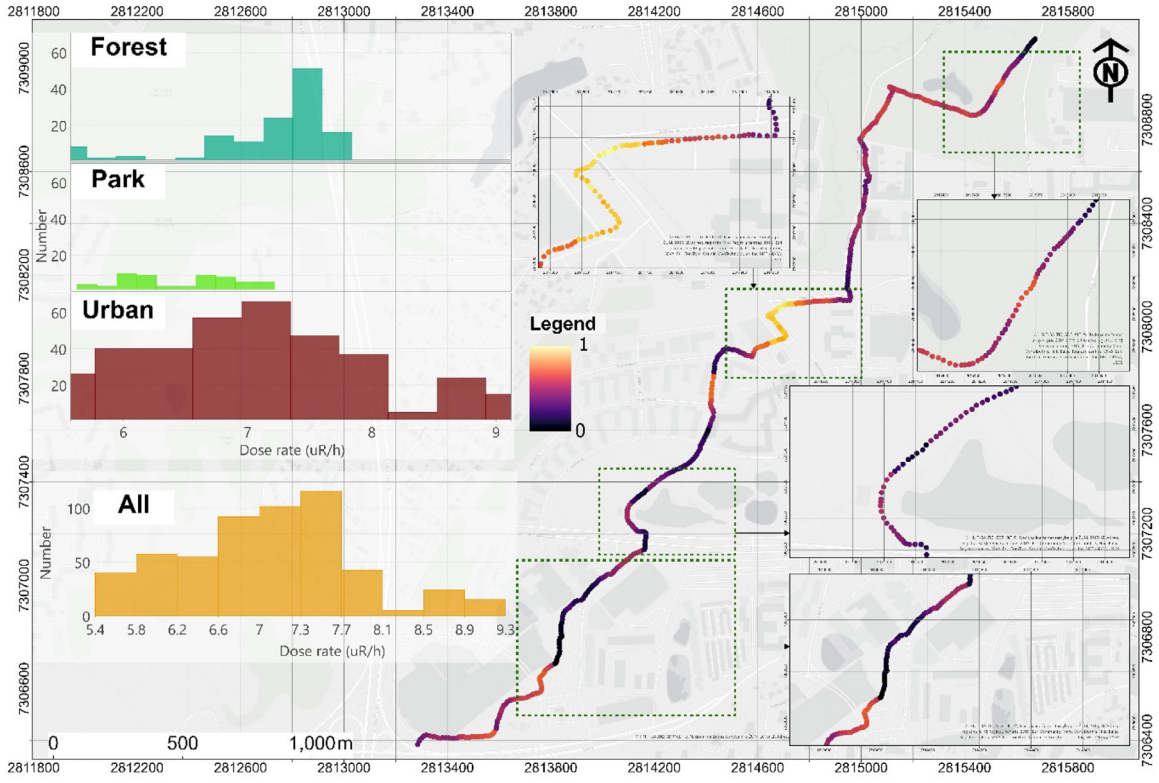


Fig. 6. Radiation dose rate in the transect studied and the respective histograms according to land use in 02-04-2025.

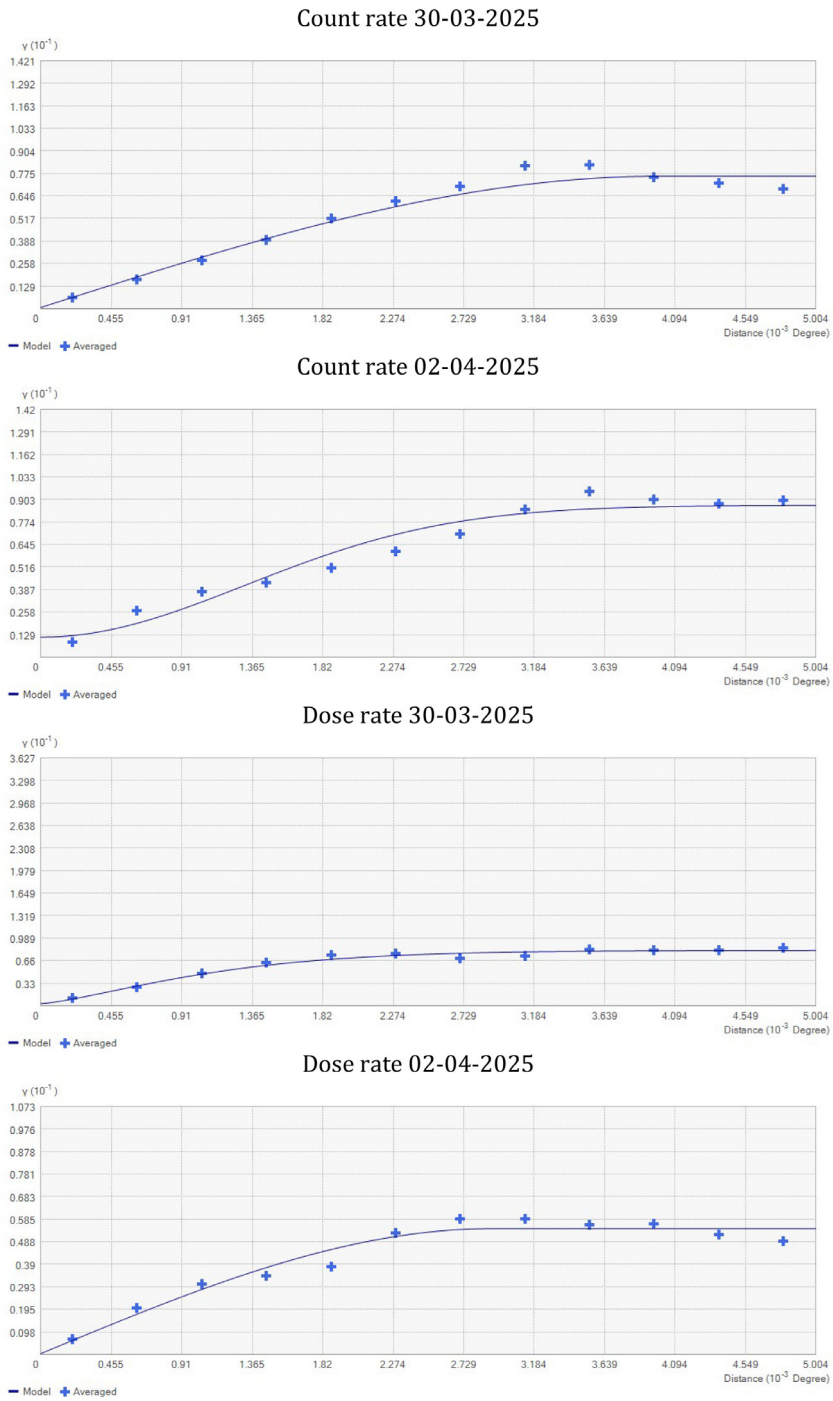


Fig. 7. Semi-Variogram results.

and dose rate on 30-03-2025 and 02-04-2025 had a significant cluster pattern, indicating that the count and dose rate concentrations are specific locations (Table 5). This was confirmed with the Getis Ord* Hot and Cold Spot analysis (Figures S4, S5, S6 and S7). On 30-03-2025, count and dose rates were high in urban areas and low in parks. On 02-04-2025, hot spots were located in urban areas and in some parts of the forest, while cold spots were observed in parks. The cluster outlier local Anselin analysis confirmed the above-mentioned except for count rate on 02-04-2025, where an HL cluster was identified. The clustered values did not have outliers showing that the low (e.g., park) and high (e.g., forest and urban) values have a specific spatial pattern. The Morans *I* scatterplot showed a high positive R^2 value in all the cases, indicating that LL and HH are very clustered and have very different values (Figures S8, S9, S10 and S11).

Table 4
Cross validation results.

	30-03-2025		02-04-2025	
	Count rate	Dose rate	Count rate	Dose rate
Mean	-0.00036	-0.00017	-0.00018	-0.00017
Root-Mean-Square Error (RMSE)	0.03577	0.07352	0.04697	0.03916
Mean Standardized	-0.0037	-0.00143	-0.00114	-0.00179
Root-Mean-Square Standardized	0.72989	0.82146	0.66980	0.86303
Average Standard Error	0.05227	0.09015	0.07302	0.04700
R^2	0.974, p<0.001	0.907, p<0.001	0.965, p<0.001	0.966, p<0.001

Table 5
Spatial autocorrelation (Global Moran's I) results.

	30-03-2025		02-04-2025	
	Count rate	Dose rate	Count rate	Dose rate
Moran's Index	0.97017	0.96672	0.96658	0.96686
Expected Index	-0.00182	-0.00182	-0.00182	-0.00182
Variance	0.00159	0.00159	0.00161	0.00160
z-score	24.31111	24.23046	24.13789	24.16780
p-value	0.00000	0.00000	0.00000	0.00000

The average dose rate values were 7.050 μR/h (0.618 mSv/y)[21] on 30-03-2025 and 7.150 μR/h (0.627 mSv/y) on 02-04-2025. The maximum value observed was in forest at 9.310 μR/h (0.816 mSv/h). The study was conducted outdoors for only two days, so more measurements are needed. We assume here that the person is moving as we conduct this work. Nevertheless, the mSv values observed are below those mentioned in Article 12 (*Dose limits for public exposure*) of the European Council Directive 2013/59/Euratom of 5 December 2013.[22] According to the directive, "public exposure" *means exposure of individuals, excluding any occupational or medical exposure*, which includes persons that circulate outdoors. Although the levels identified were low and not dangerous to human health, more studies are A: needed at different times of the day, weather conditions, or seasons in different land uses.

In this work, we illustrated the method for two sampling periods, and it is key that more measurements are needed. This will increase the robustness of the results and their contribution to urban planning by identifying areas where radiation may be harmful, especially in an area that was affected by the Chernobyl nuclear disaster. This will be important information for the municipality. The RadiaCode 103 is very useful in urban environments because of its compact nature and ease of use. If areas of high radiation emissions were found, it would be important to identify the sources of emission and collect samples (e.g., soil) to be assessed in the laboratory. As shown by the leave-one-out cross-validation, the model validation was very high (low RMSE and high R^2) for both sampling dates and values (Figure S3). Validation with field samples (e.g., soil) is also an important step that needs to be considered in the different parts of the transect in future research. A limitation to mapping radiation with the RadiaCode 103 is the mapped points are not always located in the same spot as the mapped location but nearby (e.g., ± 3 or 4 m). This may induce some problems in measuring the exact same location multiple times. This can be improved by increasing the GPS accuracy. Some recommendations when applying this methodology include: 1) walking at the same pace throughout the survey, 2) have the same person measure radiation in the field to avoid differences in walking rhythm, and 3) stop RadiaCode 103 measurements if the surveyor stops walking. This is especially important near crossroads in urban areas, where the surveyor is obligated to stop due to traffic. It is important to have the RadiaCode application recording only when walking.

Ethics statements

The work did not involve human test subjects.
The work did not involve animals.
The work did not involve data collected from social media platforms.

Declaration of competing interest

The authors declare that they have no known competing financial interests or personal relationships that could have appeared to influence the work reported in this paper.

[21] Units were converter using https://converter.eu/radiation/ converter.
[22] https://eur-lex.europa.eu/eli/dir/2013/59/oj#ntr1-L_2014013EN.01000101-E0001.

CRediT authorship contribution statement

Paulo Pereira: Conceptualization, Methodology, Investigation, Formal analysis, Resources, Data curation, Writing – original draft. **Luis Pinto:** Formal analysis, Writing – review & editing. **Miguel Inacio:** Formal analysis, Writing – review & editing. **Damia Barcelo:** Formal analysis, Writing – review & editing. **Eric C. Brevik:** Formal analysis, Writing – review & editing. **Corinne E. Brevik:** Formal analysis, Writing – review & editing.

Data availability

Data will be made available on request.

Supplementary materials

Supplementary material associated with this article can be found, in the online version, at doi:10.1016/j.mex.2025.103414.

References

[1] D. Shahbazi-Gahrouei, M. Gholami, S. Setayandeh, A review on natural background radiation, Adv. Biomed. Res. 2 (2012) 65, doi:10.4103/2277-9175.115821.
[2] E.S. Joel, M. Omeje, M. Olawole, G.A. Adeyemi, A. Akinpelu, Z. Embong, M.A. Saeed, In-situ assessment of natural terrestrial-radioactivity from Uranium-238 (238U), Thorium-232 (232Th) and Potassium-40 (40K) in coastal urban-environment and its possible health implications, Sci. Rep., 11 (2021) 17555, doi:10.1038/s41598-021-96516-z.
[3] K. Yoshimura, Air dose rates and cesium-137 in urban areas—deposition, migration, and time dependencies after nuclear power plant accidents, J. Nucl. Sci. Technol. 59 (2022) 25–33, doi:10.1080/00223131.2021.1973608.
[4] R. Rosli, N.A. Basri, N. Omar, Atmospheric trajectory analysis of Cesium-137 from proposed nuclear power plant site in Bangka Island, Indonesia, J. Phys.: Conf. Ser., 2053, 2021, doi:10.1088/1742-6596/2053/1/012010.
[5] A.N. Shhub, Assessment of Cs-137, Am-241, and Cf-252 in well logging, Health Phys. 121 (2021) 7–17, doi:10.1097/HP.0000000000001404.
[6] J.J. Steffan, E.C. Brevik, L.C. Burgess, A. Cerda, The effect of soil on human health: an overview, Eur. J. Soil Sci. 69 (2018) 159–171, doi:10.1111/ejss.12451.
[7] E. Brevik, L. Slaughter, B.R. Singh, J.J. Steffan, D. Collier, P. Barnhart, P. Pereira, Soil and human health: current status and future needs, Air Soil Water Res. 13 (2020) 1–23, doi:10.1177/1178622120934441.
[8] IAEA, Categorisation of radioactive sourcesRevision of IAEA-TECDOC-1191, Categorisation of Radiation Sources, Radiation Safety Section, Vienna, Austria, 2003.
[9] P. Allisy-Roberts, J. Williams, Gamma imaging, in: P. Allisy-Roberts, J. Williams (Eds.), Farr's Physics for Medical Imaging, Second Edition, Elsevier, Amsterdam, 2008, pp. 89–151, doi:10.1016/B978-0-12-809486-0.00004-2.
[10] T. Sandle, Gamma Radiation, in: T. Sandle (Ed.), Sterility, Sterilisation and Sterility Assurance for Pharmaceuticals, Elsevier, Amsterdam, 2013, pp. 55–68, doi:10.1533/9781908818638.55.
[11] K. Ray, M. Stick, Radiation and Health Effects, in: R.C. Gupta (Ed.), Handbook of Toxicology of Chemical Warfare Agents, Elsevier, Amsterdam, 2015, pp. 431–446, doi:10.1016/B978-0-12-800159-2.00032-4.
[12] J.R. Richter, B.B. Kasten, K.R. Zinn, Imaging and Adenoviral Gene Therapy, in: D.T. Curiel (Ed.), Adenoviral Vectors for Gene Therapy, Elsevier, Amsterdam, 2016, pp. 767–802, doi:10.1016/B978-0-12-800276-6.00031-0.
[13] J. Lilley, in: Nuclear Physics: Principles and Applications, John Wiley and Sons, Chichester, UK, 2001, p. 393.
[14] IAEA (2006) Environmental consequences of the Chernobyl accident and their remediation: twenty years of experience. Report of the Chernobyl Forum Expert Group 'Environment'. Vienna, pp. 165.
[15] A.V. Yablokov, V.B. Nesterenko, Chernobyl contamination through time and space, Ann. N. Y. Acad. Sci. 1181 (2009) 4–30, doi:10.1111/j.1749-6632.2009.04820.x.
[16] I. Labunska, S. Levchuk, V. Kashparov, D. Holiaka, L. Yoschenko, D. Santillo, P. Johnston, Current radiological situation in areas of Ukraine contaminated by the Chornobyl accident: part 2. Strontium-90 transfer to culinary grains and forest woods from soils of Ivankiv district, Environ. Int. 146 (2021) 106282, doi:10.1016/j.envint.2020.106282.
[17] I.E. Titov, V.V. Krechetnikov, R.A. Mikailova, A.V. Panov, Geoinformation decision support system for remediation of the 137Cs contaminated agricultural lands after the Chernobyl NPP accident, Nucl. Eng. Technol. 54 (2022) 2244–2252, doi:10.1016/j.net.2021.12.017.
[18] P. Pereira, E. Brevik, S. Trevisani, Mapping the environment, Sci. Total Environ. 610-611 (2018) 17–23, doi:10.1016/j.scitotenv.2017.08.001.
[19] B.S.K. Lavanya, S.N. Namitha, M. Hidayath, S.B. Prathibha, M.S. Chandrashekara, Mapping of uranium in groundwater of Mysuru district, Karnataka, India and radiation dose to the population, Nucl. Part. Phys. Proc. 341 (2023) 22–27, doi:10.1016/j.nuclphysbps.2023.09.011.
[20] G. Dubois, P. Bossew, T. Tollefsen, M. De Cort, First steps towards a European atlas of natural radiation: status of the European indoor radon map, J. Environ. Radioact. 101 (2010) 786–798, doi:10.1016/j.jenvrad.2010.03.007.
[21] P.G. Martin, S. Kwong, N.T. Smith, Y. Yamashiki, O.D. Payton, F.S. Russell-Pavier, J.S. Fardoulis, D.A. Richards, T.B. Scott, 3D unmanned aerial vehicle radiation mapping for assessing contaminant distribution and mobility, Int. J. Appl. Earth Obs. Geoinf. 52 (2016) 12–19, doi:10.1016/j.jag.2016.05.007.
[22] S. Xiong, N. Wang, Z. Fan, X. Chu, Q. Wu, S. Pei, J. Wan, L. Zeng, Mapping the terrestrial air-absorbed gamma dose rate based on the data of airborne gamma-ray spectrometry in southern cities of China, J. Nucl. Sci. Technol. 49 (2012) 61–70, doi:10.1080/18811248.2011.636550.
[23] H.I. El-Reefy, H.M. Badran, T. Sharshar, M.A. Hilal, T. Elnimr, Factors affecting the distribution of natural and anthropogenic radionuclides in the coastal Burullus Lake, J. Environ. Radioact. 134 (2014) 35–42, doi:10.1016/j.jenvrad.2014.02.020.
[24] J. Amestoy, P.Y. Meslin, P. Richon, A. Delpuech, S. Derrien, H. Raynal, E. Pique, D. Bartoux, P. Chotard, P. Van Beek, M. Souhaut, T. Zambardi, Effects of environmental factors on the monitoring of environmental radioactivity by airborne gamma-ray spectrometry, J. Environ. Radioact. 237 (2021) 106695, doi:10.1016/j.jenvrad.2021.106695.
[25] M. Alem Sultani, M. Bulko, I. Sykora, M. Müllerová, J. Masarik, P. Tonhauzer, Impacts of meteorology and mixing height on radioactive and stable aerosols in Bratislava, Slovakia Atmos. Res. 311 (2024) 107710, doi:10.1016/j.atmosres.2024.107710.
[26] M.C. Hung, Impact of meteorological factors and atmospheric particulate matter on background radiation, Radiat. Environ. Biophys. (2025), doi:10.1007/s00411-025-01121-7.
[27] Barkenow, U., Fesenko, S., Kashparov, V., Kis-Benedek, G., Matisoff, G., Onda, Y., Sanzharova, N., Tarjan, S., Tyler, A., Varga, B. (2009) Guidelines on soil and vegetation sampling for radiological monitoring. Technical reports series no. 486, IAEA, Vienna, pp. 247 pp.
[28] G. Dercon, A. Lee Zhi Yi, S. Fesenko, L. Heng, Sampling of Agricultural Soils and Plants for Radioactivity Analysis, Joint FAO/IAEA Centre of Nuclear Techniques in Food and Agriculture, Vienna, Austria, 2022, doi:10.4060/cb9304en.
[29] V. Robinson, R. Clark, S. Black, R. Fry, H. Beddow, Portable gamma ray spectrometry for archaeological prospection: a preliminary investigation at Silchester Roman town, Archaeol. Prospect. 29 (2022) 353–367, doi:10.1002/arp.1859.
[30] A. Esquivel-López, C.J. Chagas, R. Pizon, R.M. Moreira, X. Sanchez, L.D. Cunha de Paula, M. Barragan, C. Cedeno, Assessment of natural radiation in a former uranium mine: a technical capacity building development. 9th International Engineering, in: Sciences and Technology Conference (IESTEC), 2024, Panama City, Panama, 2025, pp. 1–7, doi:10.1109/IESTEC62784.2024.10820241.

[31] A. Brown, P. Franken, S. Bonner, N. Dolezal, J. Moross, Safecast: successful citizen science for radiation measurement and communication after Fukushima, Radiol. Prot. 36 (2022) S82, doi:10.1088/0952-4746/36/2/S82.
[32] J. Kenens, M. Van Oudheusden, N. Mizushima, Nonscalability of "citizen science" in post-Fukushima Japan: unpacking articulations of citizen radiation measuring organizations, Public Underst. Sci. 31 (2021) 507–523, doi:10.1177/09636625211054735.
[33] V. Lujanas, A. Mastauskas, G. Lujaniene, N. Spirkauskaite, Development of radiation in Lithuania, J. Environ. Radioact. 23 (1994) 249–263, doi:10.1016/0265-931X(94)90065-5.
[34] S. Hazarti, A.N. Baghi, H. Sadeghi, M. Barak, S. Zivari, S. Rahimzadeh, Investigation of natural effective gamma dose rates case study: Ardebil province in Iran, Iranian J. Environ. Health Sci. Eng. 9 (2012) 1, doi:10.1186/1735-2746-9-1.
[35] H.R. Ghaffari, A.H. Baghani, Y. Poureshg, H. Sadeghi, P. Babaei, B. Saranjam, E. Moradiasl, A.H. Mahvi, M. Fazlzadeh, Gamma radiation in the mineral hot springs of Ardabil, Iran: assessment of environmental dose rate and health risk for swimmers, Environ. Monit. Assess. 192 (2020) 431, doi:10.1007/s10661-020-08402-2.
[36] A. Hilal, S.A. Bangroo, N.A. Kirmani, J. Ahmed Wani, A. Biswas, M.I. Bhat, K. Farooq, O. Bashir, T.I. Shah, Geostatistical modeling—a tool for predictive soil mapping, in: S. Lamine, A. Kayad, P.C. Pandey, P.K. Srivastava, F. Muñoz-Arriola (Eds.), Remote Sensing in Precision Agriculture Transforming Scientific Advancement Into Innovation, Elsevier, Amsterdam, 2024, pp. 389–418, doi:10.1016/B978-0-323-91068-2.00011-4.
[37] A. Ziakopoulos, Spatial analysis of harsh driving behavior events in urban networks using high-resolution smartphone and geometric data, Accid. Anal. Prev. 157 (2021) 106189, doi:10.1016/j.aap.2021.106189.
[38] A.H. Wong, T.J. Kwon, Development and evaluation of geostatistical methods for estimating weather related collisions: a large-scale case study, Transp. Res. Rec. 2675 (2021) 828–840, doi:10.1177/03611981211020008.